REMARKS

This application has been reviewed in light of the Office Action dated July 12, 2004. Claims 15-29 are presented for examination. Claims 15 and 23 have been amended to define still more clearly what Applicants regard as their invention. New Claims 24-29 have been added to provide Applicants with a more complete scope of protection. Favorable reconsideration is requested.

Clarifying amendments have been made to the specification, in conformity with other portions of the specification.

According to the description appearing at page 77, lines 14-26 in the specification, the specific resistance of the carbon film is measured through observation of the carbon film by the interatomic force/funnel microscope (AFM). In the AFM, an I/V curve between the probe and the electrode is detected at each scanning point on the sample's surface. That is, at each point the resistivity from the probe to the electrode is detected.

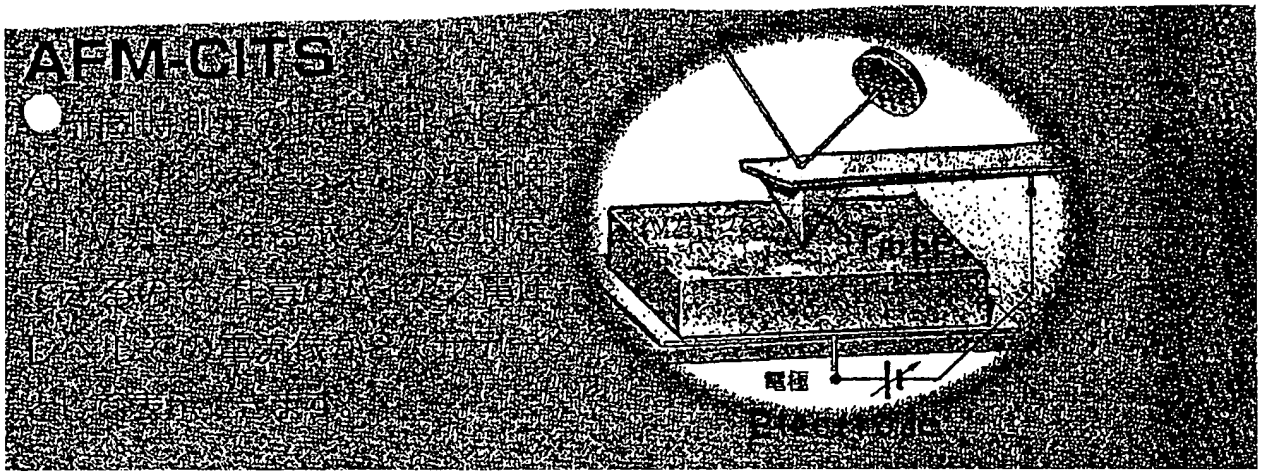

In the present invention, the conductive film corresponds to the electrode. As explained by the attached copy of the article entitled "Scanning Force/Tunneling Microscopy as a Novel Technique for the Study of Nanometer-Scale Dielectric Breakdown

of Silicon Oxide Layer", Jpn. J. Appl. Phys., Vol. 32 (1993), pp. 290-293, Part 1, No. 1B, January 1993, by Y. Fukano et al., the AFM is used to study the local dielectric breakdown for the silicon oxide layer by scanning the sample surface (see page 290, right column of the article). That is, the AFM is used to investigate the characteristics between the probe and the substrate. As can be appreciated in view of the article and the measuring method described from page 77, line 14 to page 78, line 2 of the specification, the specific resistance measured by the AFM (see page 77, lines 24-26 of the specification) is a resistivity between the probe and the conductive film. Thus, the specification has been amended to clarify that the evaluation is for a specific resistance of the carbon film in a direction taken from the probe to the electrically conductive film.

Claims 15 and 21-23 were rejected under 35 U.S.C. § 102(b) as being anticipated by U.S. Patent 5,532,544 (Yoshioka et al.). Claims 16 and 20 were rejected under 35 U.S.C. § 103(a) as being unpatentable over Yoshioka et al. in view of U.S. Patent 5,986,389 (Tsukamoto et al.).

According to an aspect of the present invention, an electron-emitting device is provided with a carbon film in which a change of a physical property of the carbon film is restrained. A description of the change in the physical property of the carbon film and how the change affects electron emission efficiency is set forth from page 27, line 18 to page 28, line 13 of the specification. The change in the physical property is a change from a less complete crystal state to a more complete crystal state in the carbon film, during driving.

From page 29, line 19 to page 30, line 14 of the specification, a description is made of one embodiment according to the present invention, in which an electron beam irradiates the carbon film during an activation step of the carbon film to promote the crystallization of the carbon film. In other words, the change of the physical property of the carbon film is accelerated for crystallization by the electron beam irradiation. A more crystallized carbon film will not change in its physical property during driving and thus stabilizes the electron emitting characteristics of the device.

The degree of the crystallization of the carbon film is represented by (and proportional to) the conductivity or resistivity (specific resistance) in the carbon film. In one embodiment of the invention, the resistivity of the carbon film is limited to "not larger than 0.001Ωm", to represent the degree of crystallization in the carbon film.

Independent Claim 15 recites an electron-emitting device comprising a first electrically conductive film, a second electrically conductive film, and a carbon film for emitting electrons disposed to cover at least a part of the first electrically conductive film. A resistivity of the carbon film is not larger than 0.001 Ωm, when an electrically conductive probe of an Atomic Force Microscope contacts a portion of the carbon film positioned over the first electrically conductive film, and when the resistivity is measured in a direction from the probe toward the first electrically conductive film.

In support of the rejection of Claim 15, the Office Action states:

"Yoshioka ('544) teaches in figure 27 and in column 14, line 10 through column 16, line 27, an electron-emitting device comprising: a first electrically conductive

film (1); a second electrically conductive film (2); and a carbon film (16) for emitting electrons disposed to cover a part of the first electrically conductive film.

The limitation of the use of an electrically conductive probe to measure the resistivity of the carbon has not been given patentable weight because it is not germane to the final structure of the device."

However, Claim 15 explicitly recites that the carbon film has a resistivity that is "not larger than 0.001Ωm" in a direction from a probe toward a first electrically conductive film. Owing to this resistivity, the carbon film inherently has a crystallized structure with a degree of crystallization corresponding to the resistivity. Applicants respectfully submit that the recited resistivity *is* a patentably distinguishing feature of the carbon film *structure*, and must be given patentable weight.[1/] Although Claim 15 further specifies a condition in which the resistivity is observed[2/] -- i.e., a case where an electrically conductive probe of an Atomic Force Microscope contacts a portion of the carbon film positioned over the first electrically conductive film, this latter recitation is not believed to negate the explicit recitation of the specific resistivity that must be given patentable weight.

Indeed, Applicants respectfully assert that nothing in Yoshioka et al. would teach or suggest that resistivity feature of Claim 15, let alone a highly crystallized carbon film in which the degree of crystallization is represented by the resistivity. Accordingly, Yoshioka et al. cannot anticipate Claim 15, since it is well established that "[a] claim is

---

1/ If the Examiner believes otherwise, he is respectfully requested to cite specific case law or Patent and Trademark Office rules in support of his position.

2/ The condition is recited because the numerical value of resistivity may depend on the manner in which the measurement is taken.

anticipated only if each and every element as set forth in the claim is found . . . in a single prior art reference." M.P.E.P. § 2131 (citation omitted). For these reasons, Claim 15 is believed to be clearly patentable over Yoshioka et al., and withdrawal of the rejection of that claim is respectfully requested.

A review of the other art relied on in the Office Action has failed to reveal anything which, in Applicants' opinion, would remedy the deficiency of Yoshioka et al. as a reference against independent Claim 15. Accordingly, Claim 15 is believed clearly patentable over that art as well.

The dependent claims each depend from base Claim 15, and also are believed to be clearly patentable over the art relied on in the Office Action, at least for the reason that each depends from a patentable base claim.

In view of the foregoing amendments and remarks, Applicants respectfully request favorable reconsideration and early passage to issue of the present application.

Applicants' undersigned attorney may be reached in our New York office by telephone at (212) 218-2100. All correspondence should continue to be directed to our

below listed address.

Respectfully submitted,

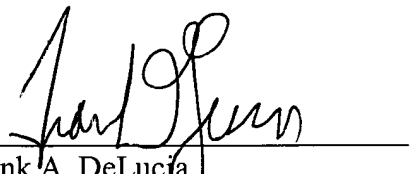

Frank A. DeLucia
Attorney for Applicants
Registration No. 42,476

FITZPATRICK, CELLA, HARPER & SCINTO
30 Rockefeller Plaza
New York, New York 10112-3801
Facsimile: (212) 218-2200

NY_MAIN 457654v1

" Attached Article"

Jpn. J. Appl. Phys. Vol. 32 (1993) pp. 290–293
Part 1, No. 1B, January 1993

Scanning Force/Tunneling Microscopy as a Novel Technique for the Study of Nanometer-Scale Dielectric Breakdown of Silicon Oxide Layer

Yoshinobu FUKANO, Yasuhiro SUGAWARA, Yoshiki YAMANISHI[1], Takahiko OASA[1] and Seizo MORITA
Department of Physics, Faculty of Science, Hiroshima University, 1-3-1 Kagamiyama, Higashi-Hiroshima, Hiroshima 724
[1]Advanced Technology Research Laboratories, Sumitomo Metal Industries, Ltd., 1-8 Fusoh-cho, Amagasaki, Hyogo 660

(Received September 12, 1992; accepted for publication November 21, 1992)

Scanning force/tunneling microscopy (AFM/STM) was proposed as a novel technique to investigate local dielectric breakdown voltage for the silicon oxide layer. It was manifested that this novel technique could simultaneously measure surface topography and distribution of dielectric breakdown voltage with nanometer-scale resolution. We confirmed that the dielectric breakdown voltage measured with the AFM/STM increased monotonously with the increase in oxide thickness. In addition to the above results, we observed that the oxide layer with visible defect had a lower dielectric breakdown voltage.

KEYWORDS: dielectric breakdown, silicon oxide layer, AFM/STM, AFM topograph, current image

1. Introduction

The silicon oxide layer plays an important role in microelectronics devices such as integrated metal oxide semiconductor (MOS) devices. In particular, dielectric breakdown characteristics of the silicon oxide layer is very important for the reliability of the devices. So far, insulating or dielectric breakdown characteristics have been investigated by fabricating a MOS capacitor.[1-3] The advantage of this technique is that it provides the statistic distribution of dielectric breakdown voltage through the entire wafer area. However, this technique has shown difficulty in characterization of the local distribution of the dielectric breakdown voltage of oxide layers with nanometer-scale resolution.

Recently, it has been reported that the dielectric breakdown voltage of the silicon oxide layer decreased with increase in the surface roughness after wet chemical processing,[4] and that surface roughness has been measured with an atomic force microscope (AFM)[5] on account of its high lateral and vertical resolution. In order to correlate surface roughness and dielectric breakdown voltage, it is necessary to investigate surface topography and local dielectric breakdown voltage simultaneously in the same area of the silicon oxide layer with nanometer-scale resolution.

In this paper, we propose a novel technique to measure the nanometer-scale distribution of dielectric breakdown voltage of the silicon oxide layer. This novel technique utilizes an AFM combined with a scanning tunneling microscope (STM),[6] namely, the scanning force/tunneling microscope (AFM/STM).[7-9] The advantage in using the AFM/STM is that it can provide both dielectric breakdown voltage and surface topography simultaneously in the same area of the sample of nanometer scale.

2. Experimental

Figure 1 shows a schematic diagram of the AFM/STM. The sample was mounted on a piezoelectric PZT tube scanner, which moved the sample in the X, Y and Z directions. The AFM topographic image was obtained by the following method. A conductive lever was put in contact with the sample surface and repulsive force was applied between the conductive lever and the sample. The value for repulsive force was obtained by multiplying the spring constant by the deflected distance of the conductive lever. Here, deflection of the conductive lever was detected with an all-fiber interferometer.[10] When the sample surface was raster-scanned, the conductive lever would deflect according to the surface topography. Servo electronics moved the sample in the Z direction to maintain constant deflection of the conductive lever. The displacement of the PZT tube scanner in the Z direction was monitored as the signal for the AFM topographic image. Local dielectric breakdown voltages were directly determined by monitoring the dielectric breakdown current I_{BD} flowing between the sample and the conductive lever when the bias voltage V_T was applied. Here, the current I_{BD} was monitored at the back side of the sample. It should be noted that this current was not a tunneling current. Because the oxide layer was much thicker than the usual tunneling gap of ~1 nm for the STM, the tunneling current would be less than 1 pA where the tunneling area was assumed to be on the order of 1 nm^2, similar to the STM. We used a conductive lever with an ion-implanted diamond tip sharpened to a radius of curvature ~100 nm[11] to detect simultaneously the force

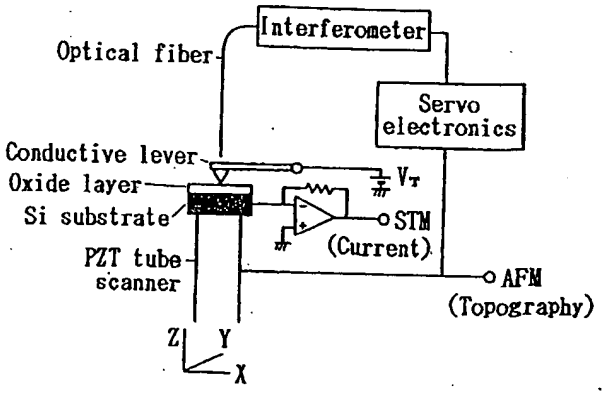

Fig. 1. Schematic diagram of simultaneous measurement with the AFM/STM. In the present study, positive bias voltage was applied to the conductive lever.

and the current I_{BD}. The conductive lever had a spring constant of $k \fallingdotseq 6$ N/m and a mechanical resonant frequency of $f_R \fallingdotseq 2$ kHz. The experimental conditions of AFM/STM measurement were as follows: repulsive force during measurement was 44~176 nN, and scanning rates of the sample for the X and Y directions were 0.4 Hz and 0.01 Hz, respectively.

3. Sample Preparation

The silicon oxide layers used in the present study were formed on p-type single-crystal Si(100) wafers. Resistivity and concentration of oxygen impurity for the wafers were 10–20 Ω·cm and $(13\text{–}15)\times10^{17}$ atoms/cm^3, respectively. At first, wafers were cleaned by means of the conventional RCA method and thermally oxidized at 950°C in dry oxygen gas. We used two types of oxide layers. One sample was observed with no further processing (as-grown oxide layer). The other sample was etch-backed to obtain a thinner oxide layer (etch-backed oxide layer). The etching process was carried out with 1% HF aqueous solution at room temperature. Thickness of the silicon oxide layers was measured with ellipsometry.

4. Results and Discussion

At first, we investigated the dielectric breakdown for the etch-backed oxide layer. The thickness of the oxide layer was estimated to be 12.5±2.4 nm. While in most cases the AFM topographic image of the surface was uniform and had no visible defect, as shown in Fig. 2(a), once we found a location where a raised defect appeared, as shown in Fig. 3(a). This defect might be formed due to the inhomogeneity of the etching rate and/or of the quality of the oxide layer. In the case of the surface without visible defect, with step increases of 2.5 V in the bias voltage, dielectric breakdown did not occur up to $V_T=10.0$ V. The AFM topographic images obtained at these bias voltages were well reproducible except for a relatively small thermal drift (~0.4 nm/min). The observable current I_{BD} flowed at $V_T=12.5$ V. From the STM current image in Fig. 2(c), we can see that the current I_{BD} flowed locally on the surface. With further increases in the bias voltage to $V_T=15.0$ V, the current I_{BD} flowed everywhere within the scanned area. We observed this local dielectric breakdown on two out of three different samples. The local dielectric breakdown may be due to inhomogeneity of the thickness or of the quality of the etch-backed oxide layer. It should be noted that, due to the small thermal drift (~0.4 nm/min), it is possible to investigate the correlation between the surface topography before dielectric breakdown, as shown in Fig. 2(a), and the STM current image after dielectric breakdown for the same area, as shown in Fig. 2(c). On the other hand, in the case of the surface with visible defect, with step increases of 2.0 V in the bias voltage, the current

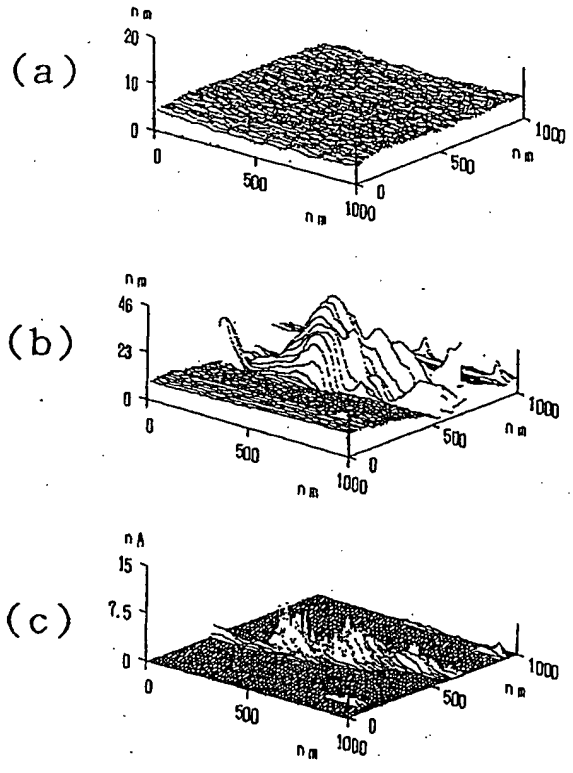

Fig. 2. Experimental results of dielectric breakdown for etch-backed oxide layer with flat surface. (a) AFM topographic image measured at $V_T=10.0$ V before dielectric breakdown, (b) AFM topographic image measured at $V_T=12.5$ V after dielectric breakdown, (c) STM current image measured simultaneously with (b).

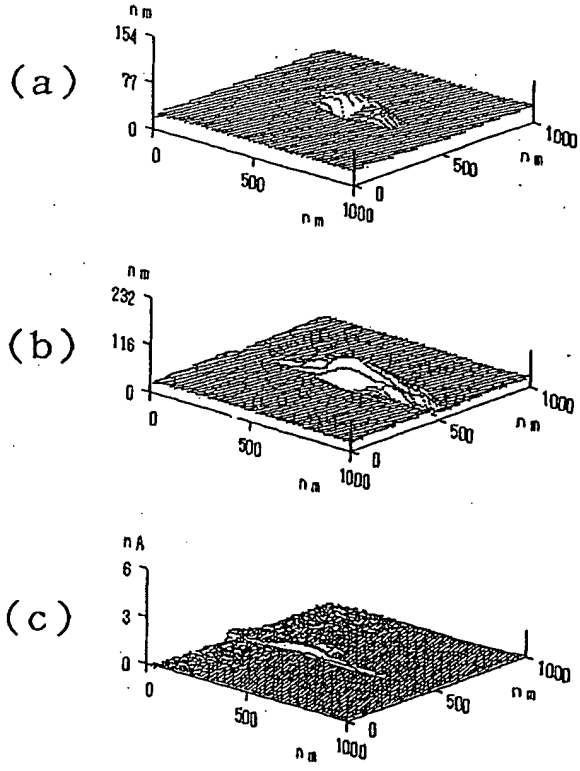

Fig. 3. Experimental results of dielectric breakdown for etch-backed oxide layer with visible defect. (a) AFM topographic image measured at $V_T=6.0$ V before dielectric breakdown, (b) AFM topographic image measured at $V_T=8.0$ V after dielectric breakdown, (c) STM current image measured simultaneously with (b).

I_{BD} flowed at V_T=8.0 V, as shown in Fig. 3(c). This dielectric breakdown voltage is 4.5 V lower than that of the oxide layer without visible defect.

Next, we investigated the dielectric breakdown for the as-grown oxide layer. Figure 4(a) shows an AFM topographic image of the as-grown oxide layer with a considerably flat surface before dielectric breakdown. The thickness of the oxide layer was estimated to be 10.5±0.7 nm. The bias voltage was V_T=10.0 V. With step increases of 2.5 V in the bias voltage V_T, the dielectric breakdown current I_{BD} flowed at V_T=12.5 V. Figures 4(b) and 4(c) show AFM topographic and STM current images after dielectric breakdown at V_T=12.5 V. From the STM current image in Fig. 4(c), we can see that the current I_{BD} uniformly flowed everywhere on the surface.

In some areas on the samples, after dielectric breakdown had occurred, dielectric breakdown current I_{BD} did not flow over a certain part of the scanned area in spite of further increases in bias voltage. These results might have something to do with the self-recovering phenomenon of a MOS structure.

From AFM topographic images in Figs. 2~4, we confirmed that the topography of the sample surface was reproducible before the dielectric breakdown. However, it changed to a rough surface after the dielectric breakdown. There are three possibilities that explain this roughening phenomenon, as follows. (1) Melting of the oxide layer may be caused by thermal heating due to high current density [~1 nA/(1 nm)^2 =10^5 A/cm^2] in the contact area [1 nm^2] of the scanned surface,[12] and recrystallization occurred immediately. (2) Contaminants may be deposited on the surface from the conductive lever by corona discharge between the conductive lever and the surface, as reported by Kaneko and Hamada.[13] (3) Electrostatic force may act between the conductive lever and the electric charge injected into the oxide layer. Barrett and Quate reported that even in the contact region, electrostatic force was observed on polished sapphire.[14] In our experiments, when the electrostatic force due to the electric charge in the oxide layer acted on the conductive lever, deflection of the conductive lever would increase or decrease. Then servo electronics drove the PZT tube scanner in the Z direction to maintain constant deflection of the conductive lever, so that an AFM topographic image was obtained as if there were large corrugation on the surface. If either (1) or (2) explains the origin of this roughening phenomenon, the scanned area before and after dielectric breakdown may differ due to the influence of thermal heating or corona discharge. Therefore, we investigated the surface at V_T=0 V after dielectric breakdown. The resulting AFM topographic image remained rough, and this roughening phenomenon was found to be irreversible. Hence, it is very difficult to estimate how the scanned area shifts between before and after dielectric breakdown. However, in the case of the etch-backed oxide layer with visible defect, it is exceptionally possible to estimate how the scanned area shifts between before and after dielectric breakdown on account of the relatively small change. Comparing Fig. 3(a) with Fig. 3(b), we can see that the dielectric breakdown area shifted toward the left by about 32 nm. This shift is smaller than the scanned width [1000 nm]. On the other hand, if (3) explains the origin of this roughening phenomenon, the electric charge might be caught by the trapping site, which has a long lifetime, so, the AFM topographic image might remain rough. In order to clarify the origin of this roughening phenomenon, further AFM/STM measurement will be required. To investigate dielectric breakdown without the roughening phenomenon, the AFM/STM measurement should be performed under constant current stress.

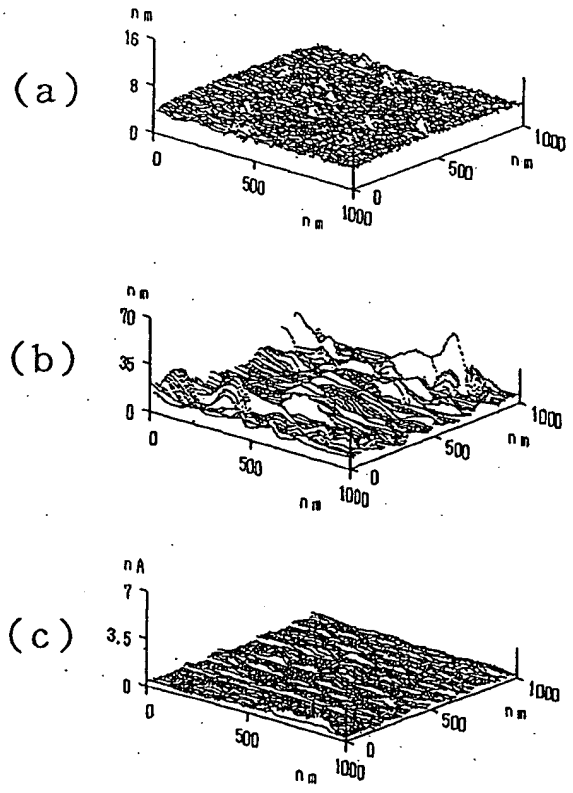

Fig. 4. Experimental results of dielectric breakdown for as-grown oxide layer with flat surface. (a) AFM topographic image measured at V_T=10.0 V before dielectric breakdown, (b) AFM topographic image measured at V_T=12.5 V after dielectric breakdown, (c) STM current image measured simultaneously with (b).

Figure 5 shows typical experimental values for the dielectric breakdown voltage measured using the AFM/STM as a function of oxide layer thickness. Here, open triangles, open circles and closed triangles correspond to etch-backed oxide layer with flat surface, as-grown oxide layer with flat surface and etch-backed oxide layer with visible defect, respectively. Lower and upper limits of dielectric breakdown voltages correspond to the points at which the dielectric breakdown current I_{BD} began to flow locally on the surface and flowed everywhere on the surface, respectively. Horizontal bars correspond to the variance of oxide layer thickness measured with ellipsometry. From Fig. 5, we confirmed that, for the as-grown and

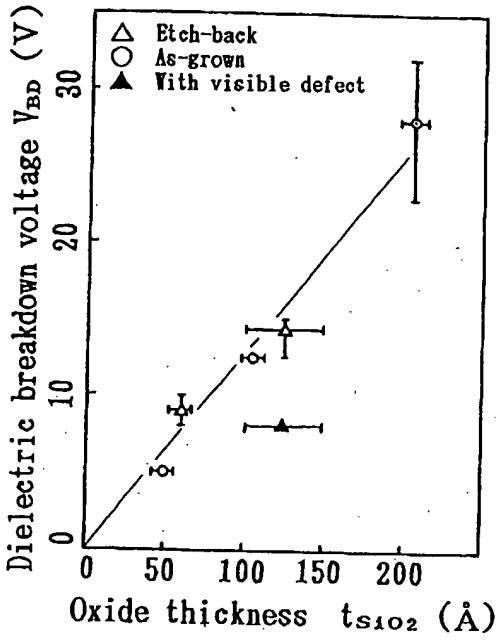

Fig. 5. Dielectric breakdown voltage of the oxide layer as a function of the oxide layer thickness. In case of the etch-backed oxide layer with visible defect, only the lowest value of the dielectric breakdown voltage is shown.

etch-backed oxide layers with flat surface, the dielectric breakdown voltage increases monotonously with increase in the oxide layer thickness. Here, deviation of the dielectric breakdown voltage from the guideline may indicate that the thickness and/or the quality of the oxide layer was not uniform. It seems that the deviation of dielectric breakdown voltage in the as-grown oxide layer is smaller than that in the etch-backed oxide layer, except for the thick oxide (20.5 nm).

We also compared the dielectric breakdown voltage at negative bias voltage with that at positive bias voltage. As a result, we found that the dielectric breakdown at negative bias voltage was always much higher than that at positive bias voltage. This result was opposite to that from the MOS capacitor measurement, where the increase in the dielectric breakdown voltage due to the depletion layer effect was dominant at the positive bias voltage. In order to explain the above opposite polarity dependence of the dielectric breakdown voltage, we considered the electric field enhancement effect, which is a well-known effect of dielectric breakdown phenomena within tip-plate capacitor in a gaseous environment.

In the MOS capacitor measurement, the electrode and silicon substrate could be regarded as parallel plates, thus the distribution of the electic field through the oxide layer was nearly uniform. On the other hand, in the AFM/STM measurement, the tip attached to the conductive lever was used as the electrode, so distribution of the electric field through the oxide layer was inhomogeneous. We conjectured that the electric field was enhanced at the tiny protrusion on top of the tip. At positive bias voltage, because of the positive streamer, this field enhancement effect seemed to decrease the dielectric breakdown voltage, overcoming the increase in dielectric breakdown voltage due to the depletion layer effect. At negative bias voltage, on the other hand, because of the negative streamer, this field enhancement effect seemed to increase the dielectric breakdown voltage.

For the quantitative comparison of the dielectric breakdown voltage obtained by means of AFM/STM measurement with that obtained by means of MOS capacitor measurement, the field enhancement effect and the depletion layer effect in the AFM/STM measurement must be taken into account.

5. Conclusions

We proposed a novel technique to investigate local dielectric breakdown voltage in air with nanometer-scale resolution. For this purpose, we used an AFM combined with a STM, that is, an AFM/STM. As a result, it was manifested that the AFM/STM could simultaneously measure the surface topography and the distribution of dielectric breakdown voltage on a nanometer scale. We confirmed that the dielectric breakdown voltage measured with the AFM/STM increased monotonously with increase in oxide thickness. Furthermore, we observed that the oxide layer with visible defect had a lower dielectric breakdown voltage.

In order to investigate the dielectric breakdown voltage of the oxide layer over a larger area, the AFM/STM should be combined with an optical microscope having an accurate stage-positioning mechanism which allows us to select the area to be scanned accurately.

Acknowledgments

We would like to thank Dr. Takao Okada, Mr. Syuzo Mishima and Mr. Syuichi Ito of Olympus Optical Co., Ltd. for the construction of the AFM/STM unit.

1) K. Hofman, G. W. Rubloff and D. R. Young: J. Appl. Phys. **61** (1987) 4548.
2) Y. Hokari: IEEE Trans. Electron Devices **35** (1988) 4212.
3) Y. Nishioka, Y. Ohji, K. Mukai, T. Sugano, Y. Wang and T. P. Ma: Appl. Phys. Lett. **54** (1989) 1127.
4) T. Ohmi, M. Miyashita, M. Itano, T. Imaoka and I. Kawanabe: IEEE Trans. Electron Devices **39** (1992) 537.
5) G. Binnig, C. F. Quate and Ch. Gerber: Phys. Rev. Lett. **56** (1986) 930.
6) G. Binnig, H. Rohrer, Ch. Gerber and E. Weibel: Phys. Rev. Lett. **49** (1982) 57.
7) Y. Sugawara, T. Ishizaka, S. Morita, S. Imai and N. Mikoshiba: Jpn. J. Appl. Phys. **29** (1990) L157.
8) Y. Sugawara, T. Ishizaka and S. Morita: Jpn. J. Appl. Phys. **29** (1990) 1533.
9) Y. Sugawara, T. Ishizaka and S. Morita: Jpn. J. Appl. Phys. **29** (1990) 1539.
10) D. Rugar, H. J. Mamin and P. Guethner: Appl. Phys. Lett. **55** (1989) 2588.
11) R. Kaneko and S. Oguchi: Jpn. J. Appl. Phys. **29** (1990) 1854.
12) U. Staufer, L. Scandella and R. Wiesendanger: Z. Phys. B **77** (1989) 281.
13) R. Kaneko and E. Hamada: J. Vac. Sci. & Technol. A **8** (1990) 577.
14) R. C. Barrett and C. F. Quate: J. Vac. Sci. & Technol. A **8** (1990) 400.